Journal of Membrane Science 383 (2011) 206–213

Contents lists available at SciVerse ScienceDirect

Journal of Membrane Science

journal homepage: www.elsevier.com/locate/memsci

Effect of zeolitic imidazolate frameworks on the gas transport performance of ZIF8-poly(1,4-phenylene ether-ether-sulfone) hybrid membranes

Kenya Díaz[a], Mar López-González[b,*], Luis F. del Castillo[a,**], Evaristo Riande[b]

[a] Instituto de Investigaciones en Materiales (UNAM), Coyoacan, México DF, Mexico
[b] Instituto de Ciencia y Tecnología de Polímeros (ICTP-CSIC), 28006 Madrid, Spain

ARTICLE INFO

Article history:
Received 14 June 2011
Received in revised form 16 August 2011
Accepted 21 August 2011
Available online 26 August 2011

Keywords:
Metal-organic frameworks
Gas transport
Selectivity
Mixed-matrix membranes
Polysulfone/ZIF-8

ABSTRACT

This work reports the permeability of hydrogen, nitrogen, oxygen, carbon dioxide, methane, ethane and ethylene across ZIF-8/poly(1,4-phenylen ether-ether-sulfone) hybrid membranes containing 0, 0.10, 0.20 and 0.30 weight fractions of ZIF-8. The glass transition temperature is independent on the filler content suggesting that the filler does not affect the polymer chains mobility. The study was carried out at 1 bar in the range of 283–313 K and the diffusion coefficient of the gases was obtained in this range of temperature by means of the lag time method. The permeability and diffusion coefficients obey Arrhenius behavior and the activation energies associated with this processes were obtained from the slopes of the respective plots. The performance of the membranes as determined by the closeness of their selectivity to the Robeson's upper bounds increases as the ZIF-8 content of the hybrid membranes increases. The membrane with 30% (w/w) content exhibits at 303 K pretty good selective properties for O_2/N_2 and H_2/N_2. The selectivity for C_2H_4/C_2H_6 is of the order of 3 with $P(C_2H_4) \cong 3$ Barrer. Extrapolation of the permeability data for H_2/N_2 at high temperatures gives a selectivity that coincides with that predicted by the Robeson limit for this pair of gases.

1. Introduction

As a result of the considerable progress that has been achieved in the use of membranes for gas separation in the last years, membrane processes are gaining larger acceptance. In the market and industry, membranes are competing in this endeavor with consolidated operations such as pressure swing absorption and cryogenic distillation. A recent review [1] highlights the most promising areas of research in gas separation. In consonance with the improvement of membranes technology, the development of efficient membranes for gas separation at high temperatures stands out. In the last decade, considerable efforts have been made in the synthesis of microporous metal-organic frameworks (MOFs) due to their potential use for gas adsorption and storage, molecular separation and catalysis [1–7]. Amid these applications, MOFs offer the possibility of being used as a material base for the preparation of membranes for gases separation. However, although novel tailored frameworks with a wide variety of structures and pore sizes as well as large surface areas have been constructed, the use of MOFs for the manufacture of continuous molecular sieve membranes for gas separation still is a challenge [8]. Zeolitic imidazolate frameworks (ZIFs), a subfamily of MOFs, have awakened great interest in this regard due to their exceptional thermal, hydrothermal and chemical stability. ZIFs consist of transition metal ions (Zn^{2+}, Co^{2+}) and imidazolate linkers which form three-dimensional frameworks resembling zeolite topologies with pore apertures of 0.2–1.5 nm [9]. The monomodal pore size distribution of ZIFs with sodalite topology, such as ZIF-7, ZIF-8, ZIF-9 and ZIF-90, make these materials special candidates for separation processes.

The preparation of continuous ZIF membranes by a simple in situ synthesis route meets serious difficulties owing to the heterogeneous nucleation of ZIF crystals on supports is very poor. To overcome this problem chemical modifications and seed coatings of the supports were performed for directing nucleation and growth of ZIF layers [8]. Using 3-aminopropyltriethoxysilane-functionalized support, Huang et al. [8] prepared ZIF-22 membranes with rather good permeation and gas separation characteristics. Li et al. [10] also reported the preparation of membranes based on ZIF-7 with a sodalite topology of about 0.3 nm pore size with promising H_2 separation abilities.

The probable fragility and high costs of molecular sieve membranes makes advisable to investigate the effect of the MOFs in gas separation by dispersing them in traditional polymers already used in the preparation of homogeneous membranes, such as polysulfones, poly(arylketones), poly(carbonates) and polyimides [11]. The preparation of mixed-matrix membranes (MMMs) containing

* Corresponding author. Tel.: +34915622900.
** Corresponding author.
E-mail addresses: mar@ictp.csic.es (M. López-González), lfelipe@unam.mx (L.F. del Castillo).

0376-7388/$ – see front matter © 2011 Elsevier B.V. All rights reserved.
doi:10.1016/j.memsci.2011.08.042

MOFs has already been reported [12,13]. Very recently, Ordoñez et al. [14] reported the permeation characteristics and ideal selectivities of pairs of gases in MMMs containing ZIF-8 dispersed in Matrimid® membranes. They found that the ideal selectivity of gas shows a great improvement above 50% (w/w) loading. This fact demonstrates a transition from a polymer-driven to a ZIF-8-controlled gas transport process.

Recently [15] the sorption and diffusion processes of carbon dioxide in poly(1,4-phenylene ether-ether-sulfone) containing ZIF-8, the weight fraction of the ZIF lying in the range $0 \leq w_{ZIF\text{-}8} \leq 0.30$, have been reported. The results showed that the solubility coefficient of CO_2 in the membranes, obtained at 303 K from sorption experiments, increases from 6.6×10^{-2} cm^3 (STP)/(cm^3 cm Hg) for the PPEES to 0.116 in the same units for the membranes with 30% (w/w) of filler content. Moreover, the diffusion coefficient of the gas as determined by pulsed field gradient (PFG) NMR spectroscopy changes from 2.1×10^{-8} cm^2 s^{-1} to 9.3×10^{-8} cm^2 s^{-1}. These results are in rather good concordance with those obtained from permeation techniques using the time lag method as well as from permeability *vs* pressure isotherms. Accordingly, the ZIF-8 filler enhances the CO_2 permeation in the MMMs membrane by increasing both the diffusivity and solubility processes. To asses the effect of ZIF-8 on the performance of the MMMs to gases separation, a thorough study was undertaken in which permeation of several gases in the membranes was measured at several temperatures. The results obtained show that ZIF-8 enhance the permeation of the gases in the membranes and, at the same time, slightly improves the permselectivity of the MMMS.

2. Experimental

ZIF-8, a zeolitic imidazolate framework containing Zn^{2+} as coordinate metal was supplied by Aldrich. Values of the particles density, particle size and BET surface area, supplied by Aldrich, were 0.35 g cm^{-3}, 4.9 μm and 1300–1800 m^2 g^{-1}. Poly(1,4-phenyleneether-ether-sulfone) (PPEES) was also supplied by Aldrich with an approximate molecular weight of 26,000 g mol^{-1} and Tg about 463 K.

The preparation of the MMMs is described in detail elsewhere [15]. Briefly, the amount of ZIF-8 necessary to prepare a MMM of desired concentration was added to a chloroform polymer solution of known composition, under strong stirring. The resulting mixture was sonicated for several time periods until an apparently homogeneous suspension was obtained. Membranes were cast onto a Teflon® mold and after casting, and in order to avoid bubbles formation, the MMM of interest was dried in vacuum at 333 K overnight, then the temperature was increased up to 473 K at intervals of 20 K, keeping the system in each step for 4 h. Finally, the membrane was cooled down to room temperature and maintained under vacuum at this temperature. The acronyms used for the MMMs thus prepared and used in the permeation studies are MMM-XX, where XX is the percentage in weight (w/w) of ZIF-8 in the composite, where the pristine polysulfone membrane will be denoted as PPEES.

The density of the dried membranes was measured by pycnometry, at 303 K, using isooctane and the results obtained for this parameter, in g cm^{-3} units, were 1.24, 1.21, 1.14 and 1.15 for PPEES, MMM-10, MMM-20 and MMM-30, respectively.

Cross-sectional surfaces of the PPEES and MMMs were sputter-coated with gold–palladium and the microscopy of the surfaces was obtained using a Philips XL 30 SEM apparatus with tungsten filament.

Differential scanning calorimetry (DSC) experiments were performed at 10 K^{-1} using a Perkin-Elmer Pyris 1 apparatus, under nitrogen atmosphere.

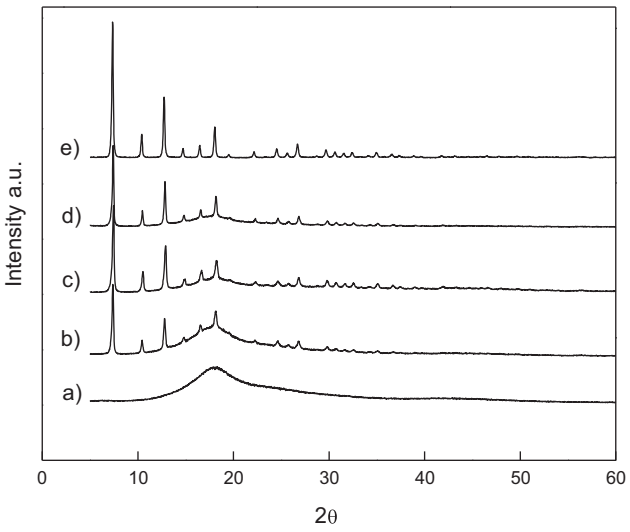

Fig. 1. X-ray patterns for PPEES (a), MMM-10 (b), MMM-20 (c), MMM-30 (d) and ZIF-8 (e).

Gas permeation across the membranes was measured with a permeation cell consisting of two compartments separated by the membrane. The cell was immersed in a water thermostat, set at the temperature of interest. Gas was allowed to flow across the membrane from the upstream chamber at pressure p_0 = 1 bar to the downstream chamber, initially at negligible pressure ($p \cong 0$). The evolution of the pressure of the gas with time in the downstream chamber, $p(t)$, was measured with a MKS 628/B pressure transducer (10^{-4}–1 mm Hg) via a PC. As usual, the $p(t)$ *vs* t isotherms present a transient process at short times followed by a straight line that defines steady-state flow behavior. The permeability coefficient was obtained from the slope of the straight line by means of the following expression

$$P = 3.59 \frac{Vl}{p_0 AT} \lim_{t\to\infty} \left[\frac{dp(t)}{dt}\right] \quad (1)$$

where V is the volume of the downstream chamber, A and l are respectively the permeation area and thickness of the membrane and T is the absolute temperature of the thermostat. Usually V, l and A are given in cgs units, the gas pressure in cm Hg and the permeability coefficient in Barrer [1 Barrer = 10^{-10} cm^3 (STP) cm cm^{-2} s^{-1} (cm Hg)$^{-1}$]. The diffusion coefficient was obtained by the time-lag method suggested by Barrer [16].

$$D = \frac{l^2}{6\theta} \quad (2)$$

In this equation, θ is the time lag, *i.e.* the time corresponding to the intersection with the abscissa axis of the $p(t)$ *vs* t straight line that describes steady state conditions. Usually, D is given in cm^2 s^{-1}. The apparent solubility coefficient of the gases in the membrane, S, was obtained from

$$S = \frac{P}{D} \quad (3)$$

S is the usually given in cm^3 (STP) cm^{-3} (cm Hg)$^{-1}$.

3. Results

X-ray diffractograms presented for the PPEES, ZIF-8, and MMMs in Fig. 1 show that the polymeric matrix does not alter the crystalline pattern of ZIF-8. In fact, only the crystalline signals strength decreases as a consequence of the decrease of ZIF-8 content in the MMMs. Moreover, the amorphous nature of the PPEES is revealed in the corresponding diffractogram.

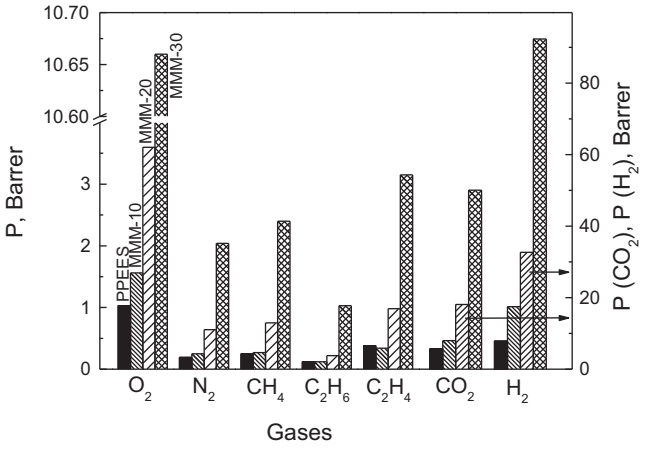

Fig. 2. Variation of the permeability coefficients for different gases at 303 K. For the sake of clarity the permeability coefficients of oxygen, nitrogen, methane, ethane and ethylene are plotted on the left-ordinate axis, and carbon dioxide and hydrogen on the right axis.

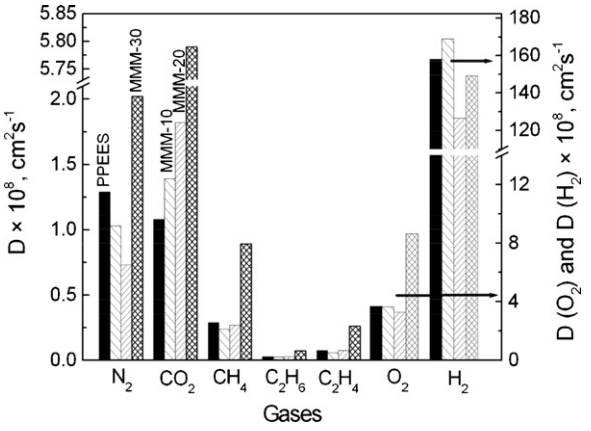

Fig. 3. Variation of the diffusion coefficient for different gases, at 303 K. For the sake of clarity, the diffusion coefficients of nitrogen, carbon dioxide, methane, ethane and ethylene are plotted on the ordinates left axis, and oxygen and hydrogen on the right axis.

The performance of MMMs for gases separation depends on the interaction polymer–filler. For example, repulsive interactions polymer–filler give rise to the formation of voids through which Knudsen flow may take place. On the other hand, favorable interactions may decrease chains polymer mobility, even at the local level, thus diminishing the gas permeability in the interface polymer–filler. Long range chains mobility affect the glass transition temperature in such a way that the larger the mobility, the lower the glass transition temperature. The Tg of the MMMs was taken as the temperature at which the low temperature side of the baseline of the DSC thermogram intersects with the slope to the middle point of the endotherm. It was found that the Tg of the MMMs is independent on the filler content. This fact suggests that strong polymer–filler interactions are absent. Knudsen flow is also absent in the MMMs because gas transport across the membrane is of diffusive type. Actually, the $p(t)$ *vs* t isotherms exhibit a transitory extending over a relatively large time, a characteristic behavior of diffusive flow.

Experimental values of the permeability coefficient of several gases across the MMMs membranes were obtained in the range of temperature 283–323 K. Illustrative plots of the permeability and diffusion coefficients of the gases H_2, O_2, N_2, CH_4, CO_2, C_2H_4 and C_2H_6 in the PPEES and the MMMs, at 303 K, are presented in Figs. 2 and 3, respectively. Using the same membrane, the error involved in the measurements depends on the values of the permeability of the MMMs in the sense that the lower is the permeability the higher the error is. For example the error involved in the determination of P for CO_2 and H_2 in the MMM-10 at 303 K is of the order of 1%. The error is of the order of 3% for N_2 and C_2H_4 and increases up to 10% for C_2H_6. As the amount of filler in the membrane increases, the error decreases. The error involved in the determination of the diffusion coefficient in MMM-10 at 303 K is of the order of 15% for all the gases. This error decreases to 7% as the amount of filler in the membranes increases up to 30%. One would expect that the departure of the transport coefficients from the averages indicated above will be larger for membranes obtained in different batches. However, this paper was only focused on the study of the effects of the amount of filler and temperature on the transport characteristics of the composite membranes. In further work, the scattering of permeability results for membranes with high filler content, obtained in different batches, will be also studied.

The permeability and diffusion coefficients as well as the apparent solubility coefficients derived from the ratio P/D, at several temperatures, are given in Tables of the Supporting Information Section. In general the permeability coefficient of the gases follows the trends $P(H_2) > P(CO_2) > P(O_2) > P(C_2H_4) > P(CH_4) \cong P(N_2) > P(C_2H_6)$. The diffusion coefficients vary in the following way: $D(H_2) \gg D(O_2) > D(CO_2) > D(N_2) > D(CH_4) > D(C_2H_4) > D(C_2H_6)$. The diffusion coefficient is closely related to the kinetic diameter of the diffusive species in such a way that in most cases the lower is the diameter the higher the diffusion coefficient is. As for the apparent solubility coefficients S, the most condensable gases exhibit the higher solubility in such a way that in most cases $S(C_2H_6) > S(CO_2) \approx S(C_2H_4) > S(CH_4) > S(O_2) > S(N_2) > S(H_2)$.

In general, the transport parameters in the MMMs increase as the percentage of filler in the MMMs augments. For example, the permeability coefficient of H_2, CH_4 and C_2H_4 at 293 K changes from 6.74, 0.21 and 0.31 for the pristine membrane to 77.82, 1.90 and 2.55 respectively for the MMM-30. In the case of light gases, the diffusive step is mainly responsible for the augment of permeability, but for condensable gases, such as CO_2 and C_2H_4, solubility is responsible for the increase.

Illustrative plots showing the temperature dependence of the permeability and diffusion coefficients of the gases are presented in Figs. 4 and 5, respectively. The plots show that the transport

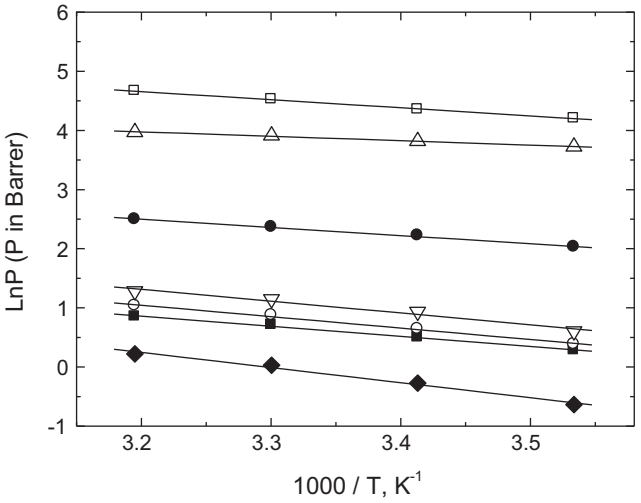

Fig. 4. Arrhenius plots for the permeability coefficients of (□) hydrogen, (△) carbon dioxide, (●) oxygen, (▽) ethylene, (○) methane (■) nitrogen and (♦) ethane in the MMM-30 hybrid membrane.

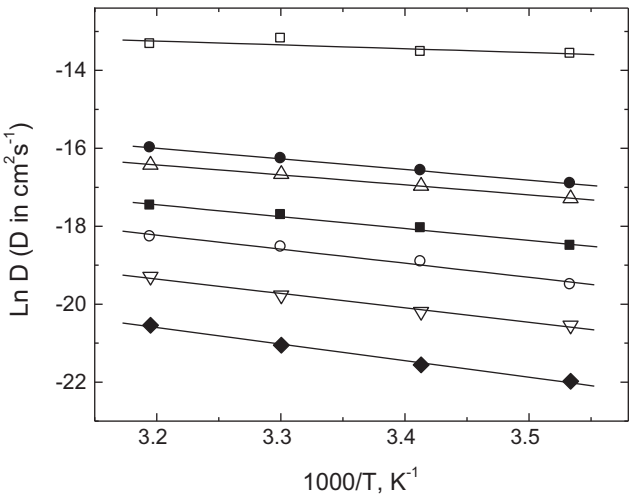

Fig. 5. Arrhenius plots for the diffusion coefficients of (□) hydrogen, (●) oxygen, (△) carbon dioxide, (■) nitrogen, (○) methane, (▽) ethylene and (♦) ethane in the MMM-30 membrane.

parameters follow Arrhenius behavior as it is the case in the transport of gases in membranes whenever phase transitions with changes in temperature do not occur. Values of the activation energies associated with the permeability and diffusion coefficients are collected in Table 1. The last column of this table collects the sorption heat of the gases in the membranes given by

$$\Delta H_S = E_P - E_D \quad (4)$$

where E_P and E_D are respectively the activation coefficients of the permeability and diffusion coefficients. The values of ΔH_S are also collected in Table 1.

Table 1
Activation energies associated with the permeability, E_P, and diffusion, E_D, coefficients. The Van't Hoff heating sorptions H_S, are also shown.

Sample	Gas	E_P, kcal/mol	E_D, kcal/mol	ΔH_S, kcal/mol
PPEES	O_2	3.48	6.46	−2.98
	N_2	4.82	7.87	−3.05
	CO_2	1.76	7.80	−6.04
	H_2	3.34	9.38	−6.04
	Methane	5.70	7.26	−1.56
	Ethylene	6.16	9.58	−3.42
MMM-10	O_2	3.67	6.60	−2.93
	N_2	4.66	8.12	−3.46
	CO_2	2.02	6.94	−4.92
	H_2	3.02	5.93	−2.91
	Methane	5.30	8.56	−3.26
	Ethane	6.03	11.54	−5.51
	Ethylene	4.89	9.27	−4.38
MMM-20	O_2	2.89	5.90	−3.01
	N_2	4.09	7.21	−3.12
	CO_2	1.48	6.33	−4.93
	H_2	2.77	3.25	−0.48
	Methane	4.21	8.69	−4.48
MMM-30	O_2	2.77	5.46	−2.69
	N_2	3.43	6.10	−2.67
	CO_2	1.50	5.12	−3.62
	H_2	2.74	1.52	1.22
	Methane	3.87	7.22	−3.35
	Ethane	5.12	8.51	−3.39
	Ethylene	3.99	7.39	−3.40

4. Discussion

The SEMs of the MMMs, presented in Fig. 6, show a rather homogeneous dispersion of the filler through the thickness of the membranes. The size of the ZIF-8 particles in the membranes is less than 1 μm suggesting that the sonication process destroys in part the aggregates of the ZIF-8 powder, whose average size lies in the vicinity of 5 μm (see Fig. 7). The crystal unit density of the filler is 0.93 g cm^{-3} whereas the diameters of the pore cavity and pore aperture are respectively 11.8 and 3.4 Å [9]. Taking for the

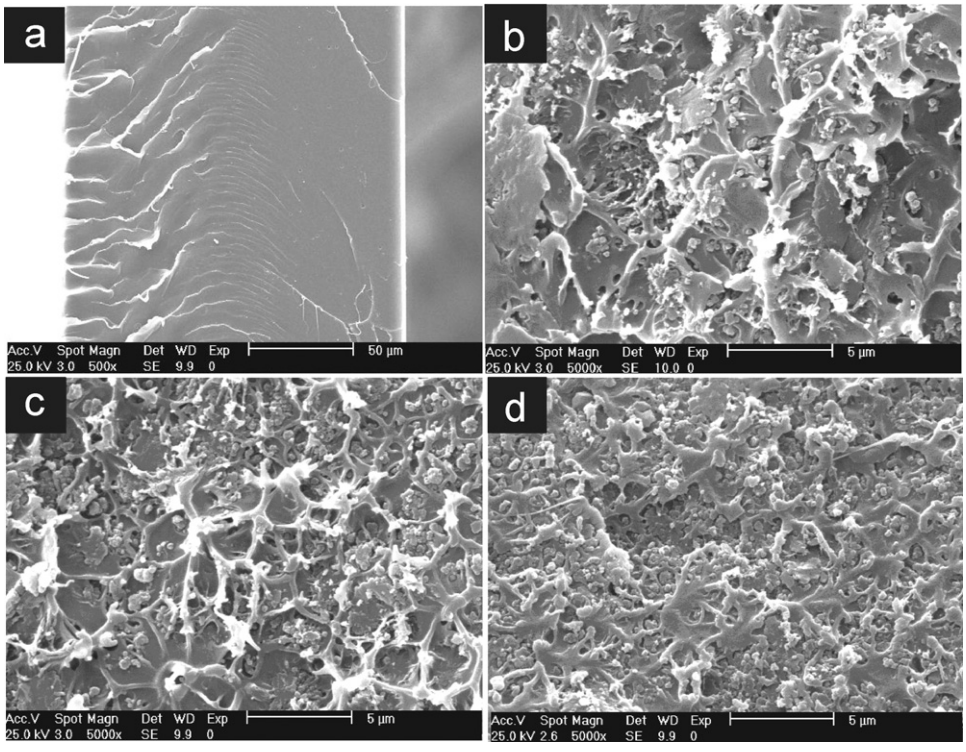

Fig. 6. SEM images showing transversal sections of (a) PPEES, (b) MMM-10, (c) MMM-20 and (d) MMM-30.

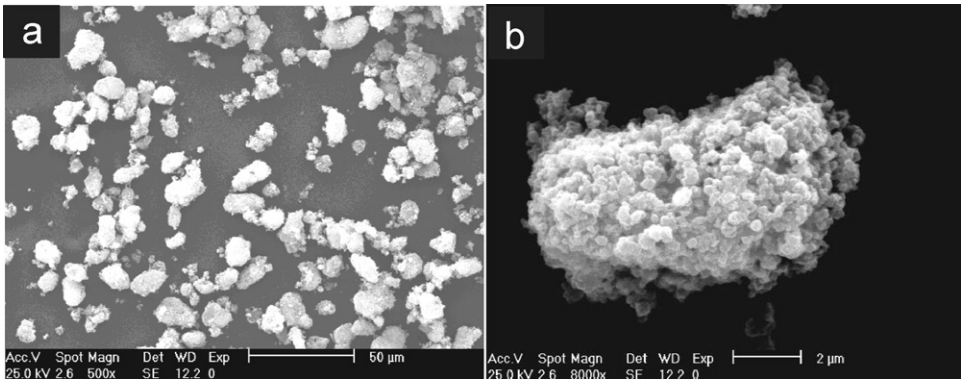

Fig. 7. SEM images for ZIF-8 particles (a) and a single particle (b).

densities of the filler and the polysulfone the values of 0.93 g cm^{-3} and 1.24 g cm^{-3}, respectively, the respective values calculated for the densities of MMM-10, MMM-20 and MMM-30 are 1.20, 1.16 and 1.13 g cm^{-3} in pretty good agreement with those measured experimentally which amount to 1.21, 1.14 and 1.15 g cm^{-3}, respectively. Then the interior of the crystalline units of ZIF-8 is presumably empty and the polymer only occupies the intercrystalline pores formed by aggregates of crystal units. Accordingly the MMMs display a variety of environments that include a continuous phase of polymer, a phase of polymer inside intercrystalline pores, a crystalline unit-polymer interface and an empty interior of crystalline units.

Earlier work [15] carried out on the sorption of CO_2 in the MMMs studied in this work show that the gas solubility increases with the filler content. The increase at low pressures proceeds in part from the augment of the concentration of gas in Langmuir sites. The interior of the crystalline units surely provides additional Langmuir sites where adsorption processes may place. As a result of the important role played by adsorption in gas sorption processes in the MMMs, both the permeability and solubility coefficients significantly decrease as pressure increases in the low pressure region. On the other hand, diffusion of $^{13}CO_2$ in the MMMs was studied by pulsed field gradient (PFG) NMR [15]. Owing to the wide variety of environments in the composite membranes, the diffusion coefficient is obtained from averages over trajectories of the diffusion species with square root mean-square end-to-end distances, $\langle r^2\rangle^{1/2}$, of 5.0, 6.0 and 6.8 μm for MMM-10, MMM-20 and MMM-30, respectively. For PPEES, the value of $\langle r^2\rangle^{1/2}$ is 0.32 μm.

The filler content increases the gas permeability in the hybrid membranes, in agreement with the results of Ordoñez et al. [14] that report similar tendency for Matrimid®/ZIF-8 membranes. These authors suggest that the ZIF-8 nanoparticles increases the distance between polymer chains, creating more free volume. Increase in free volume has also been reported for composite membranes containing fumed silica nanoparticles and silica nanoparticles as fillers [17–19]. There are cases, however, in which strong polymer–filler interactions severely reduce the molecular mobility of the matrix polymer chains and as a result loading decreases the gas permeability [20]. As indicated above, the fact that the Tg of MMMs is similar to that of the PPEES suggests that the molecular mobility is not affected by the presence of ZIF-8 nanoparticles. On the other hand, the 3.4 Å pore of the ZIF-8 crystalline unit structure selectively promotes the transport of small molecules such as H_2, O_2 and CO_2. The interpretation of the experimental permeation results of CO_2 in the MMMs in terms of the dual-mode model suggests that the ratio D_H/D_D, where D_H and D_D are respectively the diffusion coefficients in Langmuir sites and in the continuous phase, is only 0.06 for the PPEES and increases to 0.51, 0.44 and 0.22 for the MMM-10, MMM-20 and MMM-30 [15]. These results suggest that diffusion in Langmuir sites is more important in the MMMs than in the pristine membrane. In glassy membranes, local fluctuations of chains form channels that allow slippage of the diffusive particle from a cavity to a nearby one. According to Meares [21], the energy required to open a channel through which the slippage occurs is given by

$$E_D \simeq \left(\frac{\pi^2}{4}\right)\sigma^2 N_A \lambda(\mathrm{CED}) \quad (5)$$

where λ is the length of the diffusion jump, CED is the cohesive energy density, N_A is the Avogadro's number and σ is the kinetic diameter of the gas molecule that can be estimated from the Lennard–Jones collision diameter. Accordingly, in absence of phase transitions, the logarithmic plot of the diffusion coefficient against σ^2 should give a straight line. The corresponding plot for the PPEES at 303 K, presented in Fig. 9, shows that diffusion coefficient for all gases, except CO_2, fairly lies in a straight line. The linear configuration of CO_2 that makes difficult to represent this molecule by a sphere may be responsible for the disagreement observed for this gas here and in other systems. On the other hand, in spite of the heterogeneous character of the diffusive process, the plots of Fig. 8 show that the diffusion data for the MMMs also lie in straight lines. These results suggest that both the continuous phase and the interface polymer-ZIF-8 particles may control the diffusive process.

The plots of Fig. 9 show that the natural logarithm of the apparent solubility coefficient for different gases is roughly a linear function of their respective boiling temperatures at 1 bar. This is

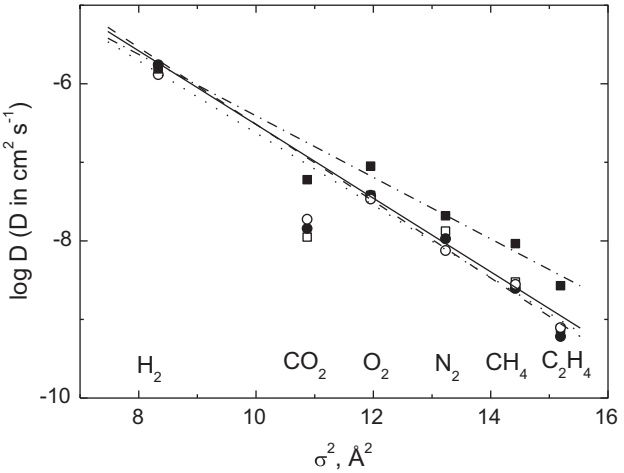

Fig. 8. Dependence of the logarithm of the diffusion coefficient (log D) at 303 K on the square of the kinetic diameter of the gases for (□) PPEES, (●) MMM-10, (○) MMM-20 and (■) MMM-30 membranes.

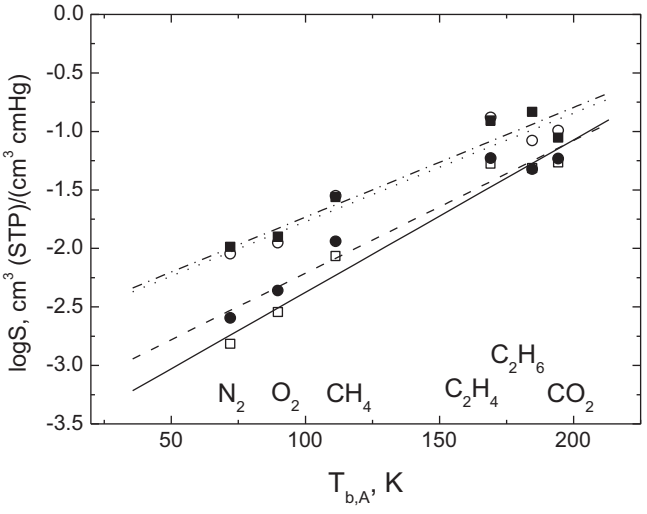

Fig. 9. Dependence of the solubility coefficient of the membranes on the boiling temperature of the gases at 1 Bar for (□) PPEES, (●) MMM-10, (○) MMM-20 and (■) MMM-30 membranes.

in consonance with the fact that neglecting enthalpic polymer-gas interactions, and in isothermal conditions, $\ln k_D \sim T_b$ where k_D is Henry's constant and T_b is the boiling temperature of the gas of interest at 1 bar [22,23]. On the other hand, gas adsorption process depends on the substrate and the chemical nature of the gas, but whatever the substrate is, gas adsorption seems to increase with gas condensability [24,25]. It is worth noting that the presence of ZIF-8 in the membranes has not a strong effect on the slopes of the $\ln S$ *vs* T_b plots.

The commercial success in the 1970s of recycling of hydrogen from ammonia purge gases (H_2/N_2) was the starting point of the penetration of membrane technology in large scale manufacturing [1]. This technology has been extended to the recovery of hydrogen from the mixture H_2/CH_4 and H_2/CO. Also oxidant and reductive atmospheres are obtained from air using membranes technology. In what follows the ideal permselectivity of the MMMs are described. The ideal selectivity of a gas A with respect to other B is currently expressed as

$$\alpha\left(\frac{A}{B}\right) = \frac{P(A)}{P(B)} = \frac{D(A)}{D(B)}\frac{S(A)}{S(B)} \tag{6}$$

where $P(A)$ and $P(B)$ are the permeability coefficients of gases A and B, respectively, while D and S are the diffusion and apparent solubility coefficients of the corresponding gases.

In Fig. 10 the evolution of $\alpha(O_2/N_2)$ with ZIF-8 loading at several temperatures is shown. It can be seen that the permselectivity does not undergo strong oscillations in the 283–313 K temperature range. In fact $\alpha(O_2/N_2)$ oscillates between 5 and 6, and loading does not seriously affect the permselectivity of the membranes. However, as the results of Fig. 10 show, loading significantly increases the membrane performances as a result of the strong increase in the permeability coefficients of the MMMs, without significantly altering the selectivity. For example, at 303 K, the ideal permselectivity coefficients of the PPEES, MMM-10, MMM-20 and MMM-30 are 5.4, 6.2, 5.6 and 5.2, respectively, and the corresponding permeability coefficients for oxygen are 1.03, 1.56, 3.60 and 10.66 Barrer, respectively. The values of the ratio $D(O_2)/D(N_2)$ for PPEES, MMM-10, MMM-20 and MMM-30 membranes are 2.9, 3.6, 4.5 and 4.3, putting in evidence that diffusive step is mainly responsible for the permselectivity of oxygen with respect to nitrogen at high loadings. The value of $\alpha(O_2/N_2)$ for the MMM-30 comes close to the upper-bound indicated by Robeson [26] for this pair of gases.

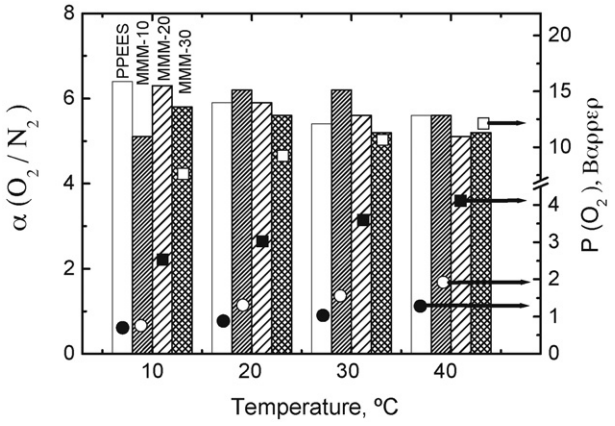

Fig. 10. Ideal selectivity of oxygen with respect to nitrogen for the membranes employed in this study, at 303 K. The open and full symbols correspond to the permeability coefficient of oxygen in each of them.

The results obtained for $\alpha(H_2/N_2)$ at different temperatures are shown in Fig. 11. At 303 K, the values of the selectivity coefficient are 41.6, 70.0, 51.0 and 45.3 for PPEES, MMM-10, MMM-20 and MMM-30, respectively. Since the permeability coefficients of hydrogen at 303 K are 7.9, 17.5, 32.7 and 92.3 Barrer, the performance of MMM-30 for the separation of hydrogen from nitrogen comes close to the upper-bound indicated by the Robeson [26] analysis for this pair of gases. The ratio of diffusion coefficients amounts to 122.6, 163.9, 173.4 and 73.91 for the PPEES, MMM-10, MMM-20 and MMM-30 respectively, and again the diffusive step is mainly responsible for the strong selectivity for hydrogen of these membranes. It should be pointed out that the determination of the diffusion coefficients of hydrogen involves large uncertainties due to the short time-lags and therefore the diffusion coefficient ratios indicated above should only be considered as semiquantitative results.

The performance of the membranes for separation of hydrogen and carbon dioxide from methane is only fair. As can be seen in Fig. 12, the values at 303 K of $\alpha(H_2/CH_4)$ for PPEES, MMM-10, MMM-20 and MMM-30 are, respectively, 31.6, 64.8, 43.5 and 38.5. These results together with the permeability coefficients of hydrogen indicated above suggest that the best performance membrane to separate hydrogen from CH_4 is the MMM-30. In spite of that, the value of $\alpha(H_2/CH_4)$ for this membrane is 51% of Robeson's upper bound for this pair of gases, but the result obtained for the permselectivity coefficient corresponding to the MMM-10 is only 17.5% of Robeson's upper bound. The values at 303 K of $\alpha(CO_2/CH_4)$ for the PPEES, MMM-10, MMM-20 and MMM-30 are 22.9, 29.5, 24.1 and

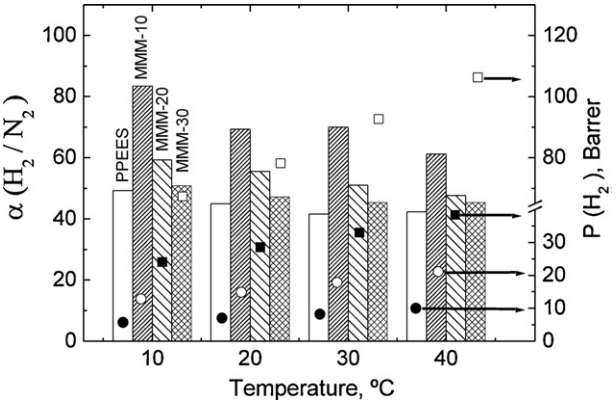

Fig. 11. Ideal selectivity of hydrogen with respect to nitrogen at 303 K. The open and full symbols correspond to the permeability coefficient of hydrogen in each of them.

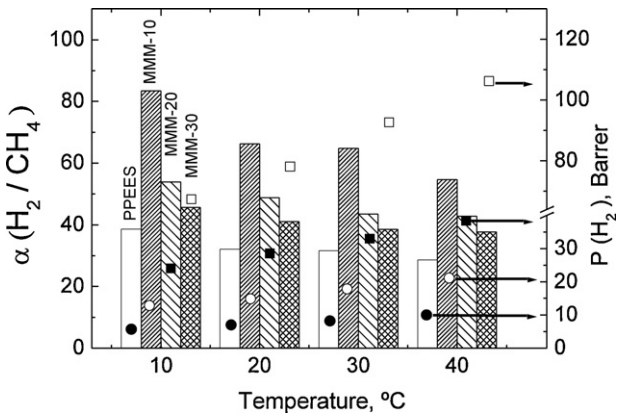

Fig. 12. Ideal separation factor of hydrogen from methane at 303 K. The open and full symbols correspond to the permeability coefficient of hydrogen in each of them.

20.8, respectively. Owing to the high permeability coefficient of the MMM-30, this hybrid membrane exhibits the better performance, though the corresponding value of $\alpha(CO_2/CH_4)$ is only 42% of the upper-bound indicated by Robeson [26] for this pair of gases with a value of $P(CO_2) = 50.0$ Barrer.

Finally, the membranes discriminate the transport of alkanes with respect to that of alkenes containing the same number of carbon atoms in the respective molecules. The values at 303 K of the permselectivity coefficient $\alpha(C_2H_4/C_2H_6)$ for the polysufones membrane, MMM-10, MMM-20 and MMM-30 are, respectively, 3.2, 2.8, 4.5 and 3.1. Since, the permeability coefficients of ethylene in the respective membranes are 0.38, 0.34, 0.98 and 3.15 Barrer, the MMM-30 exhibits the best characteristics for the separation of C_2H_4 from C_2H_6.

If the activation energy associated with the permeability coefficient of the gas A, $E_P(A)$, is lower than that of the gas B, $E_P(B)$, then the gas A is more permeable than the B across the membrane. The temperature dependence of the permselectivity coefficient is given by

$$\alpha\left(\frac{A}{B}\right) = \frac{P_{0A}}{P_{0B}} \exp\left[\frac{E_P(B) - E_P(A)}{RT}\right] \quad (7)$$

where P_0 is the permeability coefficient at infinite temperature. Since $E_P(B) > E_P(A)$ an increase in temperature decreases the selectivity coefficient. In principle, the increase in temperature also increases $P(A)$ and one could think this increase might compensate the decrease in $\alpha(A/B)$ caused by the augment of temperature. Actually, the Robeson notation $\alpha(A/B) = k^{-1/n}P(A)^{1/n}$ [26], here $n < 0$, indicates that the decrease of selectivity in the upper bound limit is associated with the increase of the permeability coefficient of the more permeable gas.

In the analysis of the gas permeability properties of ZIF-8/Matrimid® hybrid membranes, Ordoñez et al. [14] reported that the permeability coefficient increases as the ZIF-8 loading increases up to 40% (w/w). At higher loadings of 50% and 60% (w/w), the permeability decreased for all gases and the permselectivity showed improvement suggesting a transition from a polymer driven to a ZIF-8 controlled gas transport process. Our results show the same trends as those found for the ZIF-8/Matrimid® hybrid membranes in the sense that the performance of the membranes increases with the increase in ZIF-loading. Unfortunately, we do no dispose of results for MMMs with ZIF-loading above 30% (w/w).

Recently Li et al. [10] tested a novel zeolitic imidazolate framework (ZIF-7) membrane with pore size of about 0.3 nm and with promising H_2 separation abilities. At 493 K, the permeability coefficient is ~13.2 Barrer and the mixture separation factors for H_2/CO_2, H_2/N_2 and H_2/CH_4 are 13.6, 18.0 and 14.0, identical to the ideal selectivities. For comparative purposes it is tempting to get a semi-quantitative estimation of $\alpha(H_2/N_2)$ in the hybrid MMM-30 studied in this work, at 453 K. Assuming that phase transitions do not occur in the interfaces ZIF-8 nanoparticles–polymer matrix in the wide range of temperatures, extrapolation of the permeability results for nitrogen and hydrogen to 453 K can be performed using the activation energies of 14.3 and 11.4 kJ mol^{-1} for the former and latter gas, respectively, given in Table 1. It is worth noting that the activation energy of hydrogen obtained from Arrhenius plots of permeability results for the MMM-30 hybrid membrane coincides very satisfactorily with the apparent activation energy of 11.9 kJ mol^{-1} obtained by Li et al. [10] from permeation results across the ZIF-8 membrane. The extrapolated values of $P(H_2)$ and $P(N_2)$ for the MMM-30 hybrid membrane, at 453 K, are 405.7 and 12.9 Barrer, respectively. Hence the ideal selectivity of H_2/N_2 is 31.4, a value that corresponds to the Robeson upper bound for this system. In view of these results it would be desirable to investigate experimentally the performance of the MMM-30 hybrid membrane at high temperatures in further work.

5. Conclusions

The permeability and diffusion coefficient of all gases increases as the ZIF-8 loading increases. For all gases except hydrogen, the activation energy associated with the permeation process is lower than that corresponding to the diffusive one and both PPEES and MMMs exhibit an exothermic sorption process. The ZIF-8 loading increases the permeability coefficient without affecting in a significant way the ideal selectivity. As a result, the higher the ZIF-8 loading the better the membranes performance, the diffusive process being the main responsible for the selectivity of the membranes. The ideal selectivity of the MMM-30 for O_2/N_2 and H_2/N_2 at 303 K is close to that marked by the Robeson upper-bound for this pair of gases, whereas that of H_2/CH_4 and CO_2/CH_4 is about 50% of that predicted in the Robeson limit. The ideal selectivity for C_2H_4/C_2H_6 is 3 with $P(C_2H_4) = 3.15$ Barrer. Finally the activation energy of the permeability coefficient for H_2 in the MMM-30 membrane is similar to that found for this gas in ZIF-7 molecular sieves.

Acknowledgements

This work was supported by the CICYT through the grants MAT2008-06725-C03-01 and Project DGAPA IN-112109.

Appendix A. Supplementary data

Supplementary data associated with this article can be found, in the online version, at doi:10.1016/j.memsci.2011.08.042.

References

[1] P. Bernardo, E. Drioli, G. Golemme, Membrane gas separation: a review/state of the art, Ind. Eng. Chem. Res. 48 (2009) 4638–4663, and references therein.
[2] O.M. Yaghi, M. O'Keeffe, N.W. Ockwig, M. Eddaoudi, J. Kim, Reticular synthesis and the design of new materials, Nature 423 (2003) 705–714.
[3] S. Bourrelly, P.L. Liewellyn, C. Serre, F. Millange, T. Loiseau, G. Férey, Different adsorption behaviors of methane and carbon dioxide in the isotypic nanoporous metal terephthalates MIL-53 and MIL-47, J. Am. Chem. Soc. 127 (2005) 13519–13521.
[4] H. Furukawa, O.M. Yaghi, Storage of hydrogen, methane and carbon dioxide in highly porous covalent organic frameworks for clean energy applications, J. Am. Chem. Soc. 131 (2009) 8875–8883.
[5] I.J. Murray, M. Dincá, J.R. Long, Hydrogen storage in metal-organic frameworks, Chem. Soc. Rev. 38 (2009) 1294–1314.
[6] J.L.C. Rowsell, O.M. Yaghi, Strategies for hydrogen storage in metal-organic frameworks, Angew. Chem. Int. Ed. 44 (2005) 4670–4679.
[7] J.S. Seo, D. Whang, H. Lee, S.I. Jun, J. Oh, Y.J. Jeon, K. Kim, A homochiral metal-organic porous material for enantioselective separation and catalysis, Nature 404 (2000) 982–985.

[8] A. Huang, H. Bux, F. Steinbach, J. Caro, Molecular-sieve membrane with hydrogen permselectivity: ZIF-22 in LTA topology prepared with 3-aminopropyltriethoxysilane as covalent linker, Angew. Chem. Int. Ed. 49 (2010) 4958–4961.
[9] K.S. Park, Z. Ni, A.P. Coté, J.Y. Choi, R.D. Huang, F.J. Uribe-Romo, H.K. Chae, M. O'Keeffe, O.M. Yaghi, Exceptional chemical and thermal stability of zeolitic imidazolate frameworks, Proc. Natl. Acad. Sci. U.S.A. 103 (2006) 10186–10191.
[10] Y.S. Li, F.Y. Liang, H.G. Bux, W. Yang, J. Caro, Zeolitic imidazolate framework ZIF-7 based molecular sieve membrane for hydrogen separation, J. Membr. Sci. 354 (2010) 48–54.
[11] L.M. Robeson, Polymer membranes for gas separation, Curr. Opin. Solid State Mater. Sci. 4 (1999) 549–552.
[12] A. Car, C. Stropnik, K.-V. Peinemann, Hybrid membrane materials with different metal-organic frameworks (MOFs) for gas separation, Desalination 200 (2006) 424–426.
[13] Y. Zhang, I.H. Musselman, J.P. Ferraris, K.J. Balkus Jr., Gas permeability properties of Matrimid® membranes containing the metal-organic framework Cu-BPY-HFS, J. Membr. Sci. 313 (2008) 170–181.
[14] M.J.C. Ordoñez, K.J. Balkus Jr., J.P. Ferraris, I.H. Musselman, Molecular sieving realized with ZIF-8/Matrimid® mixed-matrix membranes, J. Membr. Sci. 361 (2010) 28–37.
[15] K. Diaz, L. Garrido, M. López-González, L.F. del Castillo, E. Riande, CO_2 transport in polysulfone membranes containing zeolitic imidazolate frameworks as determined by permeation and PFG NMR techniques, Macromolecules 43 (2010) 316–325.
[16] R.M. Barrer, Permeation, diffusion and solution of gases in organic polymers, Trans. Faraday Soc. 35 (1939) 628–643.
[17] T.C. Merkel, B.D. Freeman, R.J. Spontak, I. Pinnau, Z. He, A.J. Hill, P. Maekin, Sorption, transport and structural evidence for enhanced free volume in poly(4-methyl-2-pentyne)/fumed silica nanocomposite membranes, Chem. Mater. 15 (2003) 109–123.
[18] J. Ahn, W.J. Chung, I. Pinnau, M.D. Guiver, Polysulfone/silica nanoparticle mixed-matrix membranes for gas separation, J. Membr. Sci. 314 (2008) 123–133.
[19] S. Matteucci, V.A. Kusuma, S.D. Kelman, B.D. Freeman, Gas transport properties of MgO filled poly(1-trimethylsilyl-1-propyne) nanocomposites, Polymer 49 (2008) 1659–1675.
[20] T.T. Moore, R. Mahajan, D.Q. Vu, W.J. Koros, Hybrid membrane materials comprising organic polymers with dispersed phases, AICHE J. 50 (2004) 311–321.
[21] P. Meares, The diffusion of gases through polyvinyl acetate, J. Am. Chem. Soc. 76 (1954) 3415–3422.
[22] J.H. Petropoulos, Some important aspects of solubility of simple micromolecules in polymeric media, Pure Appl. Chem. 65 (1993) 219–228.
[23] M. López-González, V. Compañ, E. Riande, Langmuir sites in semicrystalline rubbery films? Macromolecules 36 (2003) 8576.
[24] R.J. Harper, G.R. Stifel, R.B. Anderson, Adsorption of gases on 4A synthetic zeolite, Can. J. Chem. 47 (1969) 4661–4667.
[25] S. Basu, P.E. Henshaw, N. Biswas, H.K. Kwan, Prediction of gas-phase adsorption isotherms using neural nets, Can. J. Chem. Eng. 80 (2002) 506–512.
[26] L.M. Robeson, correlation of separation factor versus permeability for polymeric membranes, J. Membr. Sci. 62 (1991) 165–185, The upper bond revisited, J. Membr. Sci. 320 (2008) 390–400.